Journal of Drug Delivery Science and Technology 87 (2023) 104822

Contents lists available at ScienceDirect

Journal of Drug Delivery Science and Technology

journal homepage: www.elsevier.com/locate/jddst

Bioconjugation of the gold drug auranofin to human ferritin yields a potent cytotoxin

Lucrezia Cosottini [a,b], Lara Massai [a], Veronica Ghini [a,b], Stefano Zineddu [a,b], Andrea Geri [a], Michele Mannelli [c], Silvia Ciambellotti [a,b], Mirko Severi [a], Tania Gamberi [c], Luigi Messori [a,*], Paola Turano [a,b,d,**]

[a] Department of Chemistry "Ugo Schiff", University of Florence, Sesto Fiorentino, 50019, Italy
[b] Magnetic Resonance Center (CERM), University of Florence, Sesto Fiorentino, 50019, Italy
[c] Department of Experimental and Clinical Biomedical Sciences "Mario Serio", University of Florence, Florence, 50134, Italy
[d] Consorzio Interuniversitario Risonanze Magnetiche di Metallo Proteine (CIRMMP), Sesto Fiorentino, 50019, Italy

ARTICLE INFO

Keywords:
Auranofin
Ferritin
Metal-based drugs

ABSTRACT

Ferritin may serve as a nanocarrier for the selective delivery of anticancer metallodrugs. Here, we have prepared and characterized a well-defined conjugate between the gold drug auranofin and apoferritin containing ~14 gold atoms per nanocage (HuHf@AF hereafter). Site directed mutagenesis combined with ESI MS and ICP-OES experiments revealed that gold binding occurs exclusively at cysteines 90 and 102. HuHf@AF was found to manifest potent cytotoxic properties against A2780 cancer cells and to overcome cisplatin resistance. Interestingly, we observed that HuHf@AF induced alterations in the NMR-detectable metabolome very similar to those caused by AF implying a roughly identical mode of action. Accordingly, we also show that HuHf@AF like AF metalates efficiently the C-terminal dodecapeptide of thioredoxin reductase bearing the thiol-selenol active site (this enzyme being the main intracellular target of AF). Some features of the cellular uptake of HuHf@AF and of subsequent gold release are analyzed. On these grounds, HuHf@AF is proposed as an innovative anticancer agent, with a pharmacological profile similar to free AF, where the reactivity of the gold center, its delivery and its side effects are tightly controlled by the ferritin nanocage.

1. Introduction

Auranofin (AF) is a gold drug (Fig. 1A), approved by FDA in 1985 for the treatment of rheumatoid arthritis, that is now being repurposed as an experimental anticancer agent [1–3]. The interest in auranofin and its encouraging pharmacological profile have triggered a lot of attention on gold based drugs as a source of prospective anticancer agents [4–8]. AF consists of a gold(I) center linearly coordinated to a triethylphosphine and a tetracetylthioglucose ligand. AF behaves as a typical prodrug requiring chemical activation to perform its biological actions; the first step of the activation process is the release of the thiosugar moiety [9]. AF, once activated, can bind tightly to several cellular proteins, in particular proteins containing free cysteines, thus producing its cellular effects [1–3].

Thioredoxin reductase (TrxR), a selenoenzyme that is overexpressed in various types of cancer, is reputed to be the main -though not exclusive- AF target owing to the presence of a catalytic thiol-selenol group for which the gold center manifests a very high affinity [10,11]. There are at least two confirmed forms of mammalian TrxRs with conserved structural features, i.e., the cytosolic (TrxR1) and the mitochondrial (TrxR2) one; both TrxRs play a pivotal role in protecting cells against oxidative injury. Tight binding of AF to thioredoxin reductase results into a strong inhibition of the oxidoreductase pathway and induction of severe oxidative stress [10,12,13]. Beyond TrxRs, a few additional protein targets for AF were suggested [14,15]. Reports have shown that treatment of A2780 ovarian cancer cells with AF alters significantly the overall cellular metabolism, having as a major and early effect the overproduction of glutathione [16]. Consistently, a subsequent proteomic study has shown that AF treatment in A2780 cells induces a large increase in the amounts of two enzymes involved in GSH

* Corresponding author. Department of Chemistry "Ugo Schiff", University of Florence, Sesto Fiorentino, 50019, Italy.
** Corresponding author. Department of Chemistry "Ugo Schiff", University of Florence, Sesto Fiorentino, 50019, Italy.
E-mail addresses: luigi.messori@unifi.it (L. Messori), paola.turano@unifi.it (P. Turano).

https://doi.org/10.1016/j.jddst.2023.104822
Received 17 March 2023; Received in revised form 20 July 2023; Accepted 3 August 2023
Available online 4 August 2023

biosynthesis, namely GCLC (glutamate-cysteine ligase catalytic subunit) and GCLM (glutamate-cysteine ligase regulatory subunit) [17].

The conjugation of cytotoxic metal-based drugs to selected proteins may lead to the obtainment of bioconjugates with improved pharmacological properties and more favorable systemic toxicity profiles. The case of ferritin (Fig. 1B–D) is peculiar; the reason is twofold. On one hand, the human ferritins manifest negligible toxicity and immunogenicity profiles [18]. On the other hand, the protein architecture makes it a versatile nanocarrier. The structure of the protein is that of a nanocage 24-mer of 12 nm external diameter and with octahedral symmetry, pierced by two different types of channels that connect the inner cavity (8 nm diameter) to the external bulk [19–22]. The 8 hydrophilic channels located in correspondence to the 3-fold axes drive the incorporation of small cationic metal complexes thanks to an attractive electrostatic gradient [23,24]. On the contrary, the 6 channels located at the 4-fold axes are essentially hydrophobic and are reported to trap some cations, without allowing their passage into the inner cavity [23,24]. Therefore, metal based drugs can in principle bind to the ferritin shell via multiple mechanisms: binding to solvent exposed amino acids on the internal or external surface of the protein or via interactions with amino acids at the 3- and 4-fold axes. Several examples have been reported in the recent literature [25–28].

Here, we have exploited the chance of preparing adducts between auranofin and the ferritin nanocage without disassembly. The resulting adduct (HuHf@AF hereafter) has been characterized in depth from the chemical point of view and then evaluated for its anticancer properties. Notably, in parallel to our investigation, adducts of AF with both human ferritin and horse spleen have been prepared and investigated by Lucignano et al. [29]; valuable structural information has been obtained through X-ray diffraction measurements. However, this latter study features a very different situation than ours as the adducts were obtained through the alkaline disassembly/assembly procedure, were not subjected to extensive dialysis and turned out to contain a far larger amount of associated gold, mostly present in the inner cavity [29]. This implies that their biological and pharmacological properties may be very different from those of our adducts.

2. Materials and methods

2.1. Auranofin

Auranofin was purchased from Sigma-Aldrich with the following characteristics: Code number: A6733, Purity ≥98% (HPLC).

2.2. Ferritin sample preparation

The recombinant homopolymeric human heavy chain ferritin (HuHf) was produced in *E. coli* cells following a known protocol [21,24].

Briefly, the pET-9a plasmid bearing human heavy chain ferritin gene was transformed in BL21(DE3)-pLysS competent cells. Cultures were grown in rich Luria-Bertani medium at 37 °C in the presence of kanamycin (50 μg mL^{-1}) and chloramphenicol (34 μg mL^{-1}). When the $OD_{600\ nm}$ reaches 0.6–0.8, 1 mM IPTG is added inducing the overexpression of the protein for 4 h at 37 °C. The cells were collected by centrifugation at 7500 rpm for 15 min and disrupted by sonication. Subsequently, the clarification of the lysate is performed by ultracentrifugation at 40 000 rpm for 40 min and by heating the supernatant at 65 °C for 15 min leading the undesired proteins to precipitate. The soluble fraction is subjected to anionic exchange chromatography with a linear sodium chloride gradient 0–1 M in 20 mM Tris pH 7.5 buffer (Q-Sepharose Fast Flow resin, GE Healthcare). The fractions containing ferritin are detected by SDS-PAGE and then united and loaded into a Superdex 200 HiLoad 16/600 column (GE Healthcare) for size exclusion chromatography in 20 mM Tris pH 7.5 buffer. The removal of all the metal ions is performed by repeated 5 L-dialysis, four with chelating and reducing agents (20 mM Tris, 2.5 mM EDTA, 15 mL ammonium thioglycolate pH 7.5 buffer), and four against 5 L of 20 mM Tris pH 7.5 buffer.

A sample of 5-F-Trp human H ferritin was obtained via the selective incorporation of ^{19}F into the side chain of W93 using 5-fluoroindole as the fluorinated precursor of the amino acid according to the procedure reported in Cosottini et al. [30]. The fluorinated protein (^{19}F HuHf) was expressed in *E. coli* cells by adapting the procedure reported above for the wild type protein; the only significant difference was that cells were grown in a M9 minimal medium at 25 °C overnight after the addition of the precursor.

2.3. Design and production of ferritin mutants

Three different mutants of HuHf were produced: C130A HuHf, C90AC102A HuHf and C90A HuHf. Site-directed amino acid substitution in human heavy chain ferritin was performed by PCR. The pET-9a HuHf expression plasmid was used as DNA template for the mutants, using the QuikChange II site-directed mutagenesis kit (Agilent Technologies). The DNA in the coding regions in all the protein expression vectors was analyzed for sequence confirmation (TubSeq service, Eurofins genomics).

C130A HuHf, C90AC102A HuHf and C90A HuHf were expressed in

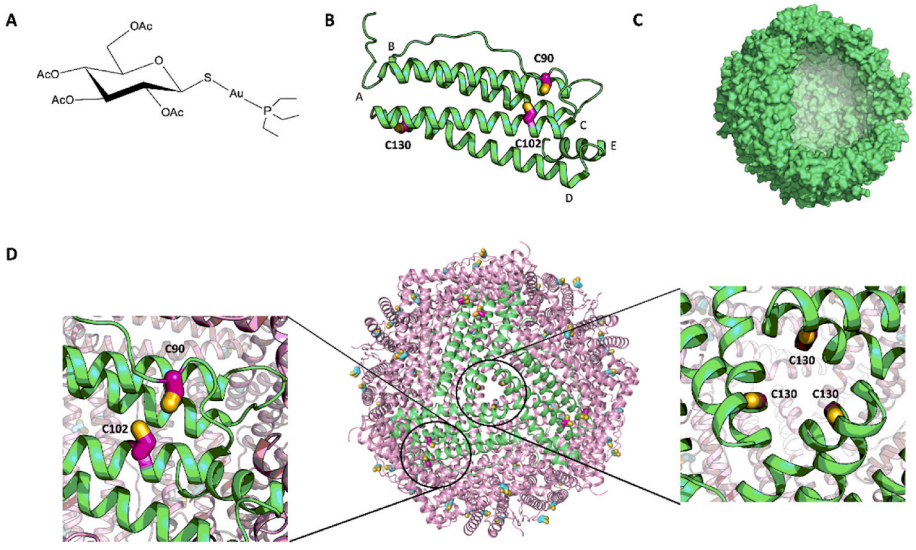

Fig. 1. A) Chemical structure of Auranofin. B) HuHf monomer (green cartoon) with cysteine residues highlighted in magenta (sticks) and α-helices named from A to E. C) 3D view of the ferritin cage showing the large inner cavity; D) external view of the ferritin nanocage: on the right close up of the C3 channel entrance (green; from the external surface to the interior) showing the three symmetry-related Cys130; on the left the close up of the two solvent-exposed Cys90 and Cys102. PDB: 4Y08. (For interpretation of the references to color in this figure legend, the reader is referred to the Web version of this article.)

BL21-DE3 pLysS *E. coli* cells following the same protocol as for the wild type (see ferritin sample preparation, paragraph 2.2).

2.4. ESI MS experiments

The protein solutions were further diluted with a 20 mM ammonium acetate solution, pH 6.8, to a final protein concentration of 5×10^{-6} M. 1% v/v of LC-MS grade formic acid was added just before infusion in the mass spectrometer. The ESI mass spectra were acquired through direct infusion at 7 μL min-1 flow rate in a TripleTOF® 5600+ high-resolution mass spectrometer (Sciex, Framingham, MA, U.S.A.), equipped with a DuoSpray® interface operating with an ESI probe.

The ESI source parameters were as follows. HuHf: positive polarity, Ionspray Voltage Floating 5500 V, Temperature 0, Ion source Gas 1 (GS1) 40 L/min; Ion source Gas 2 (GS2) 0; Curtain Gas (CUR) 20 L/min, Declustering Potential (DP) 30 V, Collision Energy (CE) 10 V, acquisition range 650–3300 *m/z*.

The mixture of HuHf@AF and C-terminal dodecapeptide of TrxR (dTrxR) was separated by centrifugation at 3000 rpm for 10 min twice using VIVASPIN 2 (Sartorius Stedim Biotech Gmbh) with a cut-off of 30 kDa.

The ESI source parameters were as follows. dTrxR: positive polarity, IonSpray Voltage Floating 5500 V, Temperature 0, Ion source Gas 1 (GS1) 30 L/min; Ion source Gas 2 (GS2) 0; Curtain Gas (CUR) 25 L/min, Declustering Potential (DP) 200 V, Collision Energy (CE) 10 V, acquisition range 1090–2000 *m/z*.

For acquisition, Analyst TF software 1.7.1 (Sciex) was used, and deconvoluted spectra were obtained by using the Bio Tool Kit micro-application v.2.2 embedded in PeakViewTM software v.2.2 (Sciex).

2.5. ICP-OES measurements

Samples were treated with 100 μL of suprapure HNO_3 recovered by sub-boiling distillation and 100 μL of suprapure HCl (30%). After dissolution, samples were diluted to a final volume of 5.0 mL with ultrapure water (UHQ – resistivity >18 MΩ cm – Milli-Q system by Millipore, Billerica, MA). Au concentrations were determined in triplicate by a Varian 720-ES axial inductively coupled plasma optical emission spectrometer (ICP-OES). Each sample was spiked with 100 μL of a 50 mg L^{-1} Ge solution used as an internal standard prior to the analysis. The introduction system consisted of a concentric pneumatic nebulizer and a cyclonic spray chamber. Calibration standards were prepared by gravimetric serial dilution from commercial stock standard solutions of Au at 1000 mg L^{-1} (Honeywell Fluka). Wavelengths used for Au determination were 242.794 and 267.594 nm, whereas for Ge the line at 209.426 nm was used. Maximum signal intensity was obtained optimizing the operating conditions. Between each sample, a solution composed by 2% v/v of HNO_3 was used.

2.6. Stability test

HuHf@AF 1:10 (HuHf-subunit/AF) was subjected to the following tests to characterize its stability.

Stability over time: ESI-MS spectra were acquired at three different time points i.e. immediately after the sample preparation (T = 0), after 2 weeks and after 1 month. Two sets of experiments were acquired; in one set in between the experiments the samples were stored at 4 °C, in the other set the samples were maintained at 37 °C.

Stability in the presence of glutathione: HuHf@AF was incubated with an excess of glutathione (10:1 M ratio with respect to Auranofin) at 37 °C. ESI-MS spectra were recorded at different time points i.e. after 1 h, after 4 h and after 24 h of incubation.

Stability in the presence of human serum albumin (HSA): HuHf@AF (WT and C90A) was incubated with HSA (1:1 M ratio with respect to ferritin subunit) at 37 °C. ESI-MS spectra were recorded at different time points i.e. T = 0 h and T = 24 h.

Stability in the presence of TrxR dodecapeptide: HuHf@AF 1:10 was incubated with dTrxR at 37 °C (1:1 with respect to the gold(I) concentration per ferritin subunit, i.e. 0.4 μM). ESI-MS spectra were recorded at T = 0 and after 5 h of incubation (T = 5 h).

2.7. Metal release at pH 4.5

ESI-MS spectra were acquired at four different time points i.e. immediately after the sample preparation (T = 0), after 1, 3, 20 h. In between the experiments the samples were maintained at 37 °C.

2.8. Cell culture

A2780 human ovarian cancer cell line (Lot N°CSC-C9491J) and A2780 cisplatin resistant (A2780cis, Lot N° CSC-9492J) cell line, were purchased from Creative Bioarray (NY 11967, USA), and were used as *in vitro* models of ovarian cancer. Cells were maintained in RPMI1640 (Euroclone, Milan, Italy) medium supplemented with 10% FBS, 1% glutamine and 1% antibiotics at 37 °C and sub-cultured twice weekly. Split 1: 5 (3–6 × 10^4 cells per cm^2).

2.9. Cytotoxic effect on A2780 cell lines

The inhibition of cell proliferation by AF and HuHf@AF on A2780 cell lines was evaluated through MTT (3-(4,5-dimethylthiazol-2-yl)-2,5-diphenyltetrazolium bromide) test at 72 h. Viable cells can convert MTT (Merck Life Science) into formazan, which is blue-colored and detectable at 595 nm. Exponentially growing cells were seeded in 96 well-microplates at a density of 5×10^4/mL and after 24 h AF, HuHf@AF and apo-HuHf were added in fresh RPMI medium at concentrations ranging from 0.0007 to 25 μM and incubated for 72 h. On the day of the test, cells were treated with 0.5 mg/mL MTT for 1 h at 37 °C. Following precipitation, blue formazan was dissolved in DMSO, and the optical density was read at 595 nm in a microplate reader interfaced with Microplate Manager/PV version 4.0 software (BioRad Laboratories, Hercules, USA). From the absorbance measurements, the half-maximal inhibitory concentration (IC_{50}) value of each compound was calculated using GraphPad Prism software version 6.0 (Graphpad Holdings, LLC, USA). The experiments were conducted both on the A2780-sensitive and A2780-resistant cells.

2.10. Sample preparation for NMR-based metabolomics

A2780 cells were seeded in 60 cm^2 tissue-culture plates at 1.8×10^5 cells/mL (total volume 10 mL) and incubated for 24 h, then exposed to concentration of the AF (diluted in DMSO) or HuHf@AF equal to 72 h-exposure IC_{50} values. The A2780 cells were also treated with apo-HuHf, at the same ferritin concentration as in the corresponding experiments with HuHf@AF. The A2780 control cells were treated with an equal concentration of DMSO. The final DMSO amount in the growth media was 0.1% of the total volume; this concentration of DMSO in A2780 culture has been reported neither to induce apoptosis nor to activate caspases. The incubation was stopped at 24 h; at the end of incubation 1–2 mL of the medium was collected for the metabolomic analysis, the cells were washed three times with PBS and then scraped in PBS supplemented with a protease-phosphatase inhibitor cocktail diluted in DMSO (Sigma-Aldrich). In agreement with procedures for NMR sample preparation cells were lysed by sonication in ice and then centrifuged at 200 000g, 30 min, 4 °C. All the samples were stored at −80 °C.

At the moment of the NMR analysis, frozen samples were thawed at room temperature and shaken before use. For cell lysates, 55 μL of ^2H_2O were added to 495 μL of each lysate sample. In the case of cell culture media, an aliquot of 300 μL of sodium phosphate buffer (70 mM Na_2HPO_4; 20% v/v ^2H_2O; 4.6 mM TMSP, pH was adjusted to the final value of 7.4 using 1 M HCl) was added to 300 μL of each medium sample. The mixtures were homogenized by vortexing for 30 s and transferred

into 5 mm NMR tubes (Bruker BioSpin srl) for analysis.

2.11. ^{1}H NMR spectroscopic experiments for metabolomics

NMR-based metabolomic analysis was performed according to standard procedures [31,32]. ^{1}H NMR spectra were recorded with a Bruker 600 MHz spectrometer, (Bruker BioSpin) optimized for metabolomic analysis, operating at 600.13 MHz proton Larmor frequency and equipped with a 5 mm PATXI ^{1}H–^{13}C–^{15}N and ^{2}H-decoupling probe including a z-axis gradient coil, an automatic tuning-matching (ATM) and an automatic refrigerated sample changer (SampleJet, Bruker BioSpin). A BTO 2000 thermocouple served for temperature stabilization at the level of approximately 0.1 K of the sample.

Before measurement, to equilibrate temperature at 300 K, samples were kept for at least 5 min inside the NMR probe head.

The cell lysate samples were acquired with the Carr–Purcell– Meiboom–Gill (CPMG) sequence using a one-dimensional (1D) spin-echo sequence with water presaturation. 512 scans, 73 728 data points, a spectral width of 12 019 Hz and a relaxation delay of 4 s were used.

The growth media were acquired with a 1D nuclear Overhauser enhancement spectroscopy (NOESY)-presaturation pulse sequence. 64 scans, 98 304 data points, a spectral width of 18 028 Hz and a relaxation delay of 4 s were used.

The raw data were multiplied by a 0.5 Hz exponential line broadening before applying Fourier transform. Transformed spectra were automatically corrected for phase and baseline distortions and calibrated at the doublet of Ala at 1.49 ppm using TopSpin 3.6 (Bruker Biospin srl).

2.12. Statistical analysis

All NMR data analyses were performed using the "R" software. Principal component analysis (PCA) was used as an exploratory analysis to obtain an overview of the sample fingerprints and to detect the presence of clusters. PCA was applied on binned NMR spectra. To this aim, each spectrum in the region 10.00–0.2 ppm was divided into 0.02 ppm chemical shift bins, and the corresponding spectral areas were integrated using the AMIX software (Bruker, Biospin srl). The area of each bin was normalized to the total spectral area, calculated with exclusion of the water and DMSO regions (4.50–5.00 ppm and 2.90–2.60 ppm, respectively). No scaling method was applied on the data.

The metabolites, whose peaks in the spectra were well resolved, were assigned and their levels analyzed using a R script developed in-house. We could identify and quantify 30 metabolites in the cell lysate spectra and 28 in the growing medium spectra. The assignment was performed using an internal ^{1}H NMR spectral library of pure organic compounds (BBIOREFCODE, Bruker BioSpin srl), public databases such as the Human Metabolome Database, stored reference NMR spectra of metabolites and literature data. Matching between new NMR data and databases was performed using the AMIX software (Bruker BioSpin srl).

The nonparametric pairwise Wilcoxon–Mann–Whitney test was used for the determination of the meaningful metabolites; a p-value <0.05 was considered statistically significant. Log_2 Fold change (FC) was calculated for each metabolite to display how the metabolite levels vary upon the different comparison. FC is calculated as the median of the ratio of the metabolite concentrations in the spectra of the two paired samples (treated vs. control). In the growth media, the metabolites were divided into two different classes, i.e. those that are taken up from the medium and those that are released into the medium. For the molecules that are released, lower/higher concentration levels upon treatment mean a lower/higher release, while for the molecules that are taken up from the growth media, lower levels upon treatment mean a greater consumption of nutrients, i.e. increased uptake, and *vice versa* for higher levels.

2.13. ^{19}F NMR spectroscopy

The cellular uptake of ferritin was analyzed by acquiring ^{19}F NMR spectra of growth media of A2780 cells treated with apo ^{19}F HuHf or ^{19}F HuHf@AF; The decrease of the ^{19}F protein signal was followed at different time points up to 1 h of treatment. One dimensional spectra were recorded at 298 K on a Bruker Avance III spectrometer operating at 14.1 T equipped with a SEL ^{1}H High Power 5 mm probe, using a zg pulse sequence, with a recycle time of 3 s, an acquisition time of 0.57 s and a total number of scans of 24 k [30].

3. Results and discussion

3.1. Preparation and chemical characterization of the bioconjugate

The loading of human heavy chain ferritin (HuHf) with AF was successfully achieved by the simple addition of a molar excess of AF with respect to HuHf-subunits in PBS, followed by stirring at 37 °C for 3 h and extensive dialysis. This method has the advantage of not requiring any cage disassembly/reassembly [27,33–35]. At the end of the process, the formation of stable bonds between the metal complex and the ferritin subunits was documented by ESI MS measurements [36]. In turn, ICP-OES analysis was used to quantitate the amount of the metal bound to the protein cage.

Several conditions were tested featuring different protein to AF molar ratios, typically ranging from 1:6 up to 1:100 HuHf-subunit/AF (Table S1). The 1:10 stoichiometry turned out to be the best condition upon considering the amount of the used metal complex and its overall solubility; the effective amount of gold in the ferritin cage resulted to be 13.8 ± 3.8 gold atom/cage. This preparative procedure turned out to be highly reproducible. The obtained ESI MS spectra show that AF binds the protein under different forms (Fig. 2A). With the 1:10 ratio, peaks corresponding to protein binding of Au(I), $[AuPEt_3]^+$, and (Au(I) + $[AuPEt_3]^+$) fragments were identified; the relative ratios of these metalated species to the apo-HuHf subunit are as reported in Fig. 2B.

3.2. Stability of the bioconjugate

The stability of the adducts over time was tested until 1 month from the reaction time (T = 0). In between the experiments the samples were maintained at 4 °C (Fig. 2C and Fig. S1A); the same behavior was obtained maintaining the sample at 37 °C (data not shown). Interestingly, treatment of HuHf@AF with an excess of glutathione (10:1 M ratio with respect to Auranofin) did not cause any appreciable changes in the ESI MS spectra even after 24 h incubation, supporting its substantial stability in a GSH-rich environment (Fig. 2D and Fig. S1B). Analogously, no binding to human serum albumin (HSA) is detected in competition binding experiments conducted with a 1:1 HuHf monomer/HSA ratio at 37 °C after 24 h of incubation (Fig. S2). It is worth reminding that HSA is one of the primary ligands of auranofin in the blood thanks to its free Cys 34, which binds soft metal ions, including gold(I). Therefore, the tight association with HSA, that was reported to greatly reduce the bioavailability of AF [37–39], might be at least partially overcome by strong binding of AF to HuHf. The peculiar stability of HuHf@AF with respect to free Cys-containing molecules has been further investigated by site directed mutagenesis studies (see below).

3.3. Site directed mutagenesis

Literature data suggest that free cysteines are the favored anchoring sites for gold containing fragments in proteins [40,41], Notably, each H-ferritin subunit possesses three cysteines, i.e., Cys90, Cys102 and Cys130, all existing in their reduced SH form. Cys90 and Cys102 are located on the solvent-exposed BC-loop and C-helix respectively, while Cys130 is present at the entrance of the C3 channel (Fig. 1). Site directed mutagenesis experiments (Fig. S3) were carried out on these cysteines to

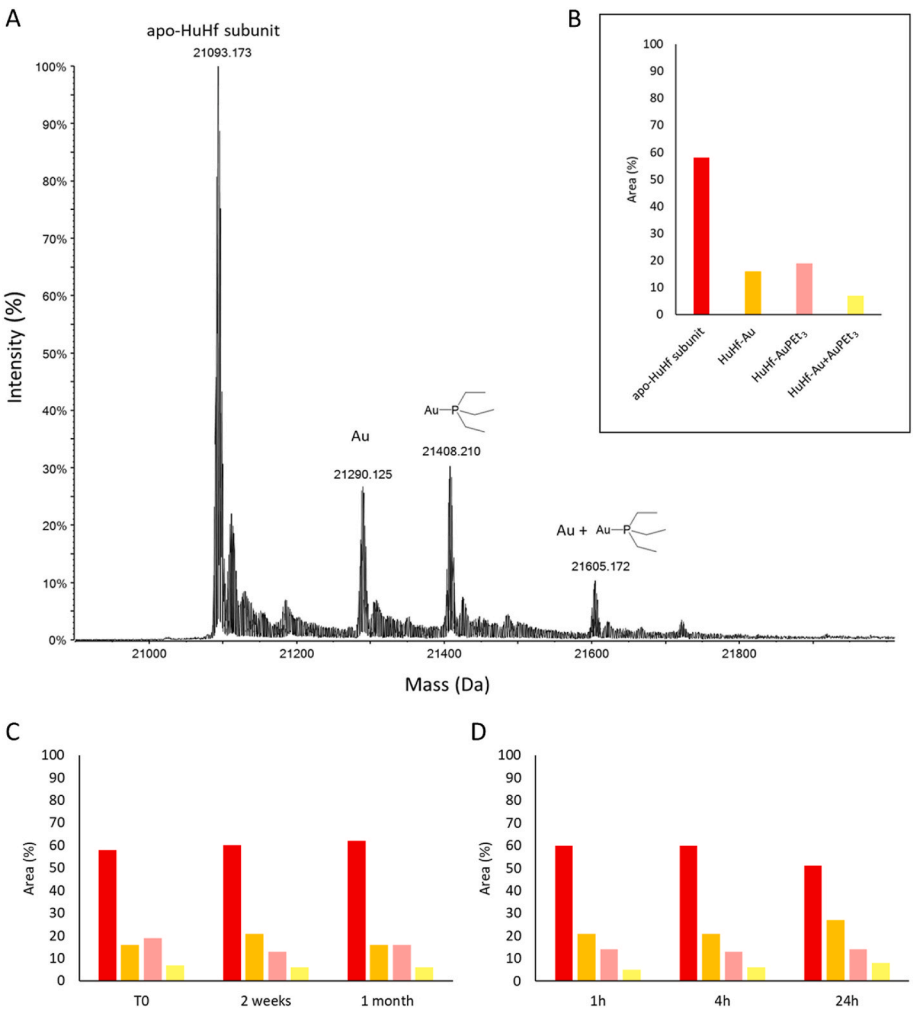

Fig. 2. HuHf@AF 1:10 A) Deconvoluted ESI MS spectrum; B-D). Bar plots of the percentage ratio of area among the apo-HuHf subunit and the differently metalated- HuHf subunits by auranofin: B) HuHf@AF 1:10; C) Stability test over time, HuHf@AF alone at T = 0, T = 2 weeks, T = 1 month. Samples were stored at 4 °C in between the experiments; D) Stability test over time of HuHf@AF incubated with an excess of glutathione at 37 °C (10:1 M ratio with respect to AF) for different time: after 1 h, after 4 h, and after 24 h.

localize unambiguously the gold binding site(s). Remarkably, replacement of Cys130 with Ala did not produce any alteration in the gold binding ability of the protein as assessed by ICP-OES and ESI MS measurements; in contrast, the double mutant C90AC102A turned out to manifest a complete loss of the gold binding ability (Fig. 3 A-C). This result demonstrates very clearly the role of cysteines 90 and 102 as the exclusive anchoring sites for gold atoms. As a further confirmation the C90A mutant, where only one of the two solvent exposed Cys is present, shows half the gold binding affinity (~7 gold atoms per cage) and a lower stability of the adduct when incubated with HSA for competition binding (see Fig. S4), thus highlighting the cooperative role of C90 and C102 in binding the gold atoms. It is worth mentioning that human serum ferritin is mostly composed of light chain subunits (HuLf) [42,43], where C90 and C102 are replaced by E90 and A102; thus, circulating ferritin should not affect the transport of HuHf@AF. Notably, our results are partially consistent with the crystallographic results reported by Lucignano et al. pointing out that gold is associated to the three cysteines but with a relatively low occupancy [29].

3.4. In vitro cytotoxic characterization

Afterwards, the cytotoxic activity of HuHf@AF was measured via a comparative determination of the half-maximum inhibitory concentration (IC_{50}) at 72 h in A2780 ovarian cancer cells, treated with HuHf@AF or free AF, by MTT test (Fig. 4). Fig. 4A–C summarizes the obtained results. Notably, both AF formulations produced potent cytotoxic actions in A2780 cells, with HuHf@AF (IC_{50} 0.26 ± 0.02 μM; Fig. 4B) being more active than free AF (IC_{50} 0.8 ± 0.21 μM; Fig. 4A) by a factor ~3. To exclude any cytotoxicity related to the cellular treatment with ferritin itself, the MTT assay was repeated, using apo-HuHf at the same concentration of HuHf@AF, at 24, 48 and 72 h (Fig. 4C). These results are very important as they point out that binding of AF to the ferritin nanocage does not cause loss of its biological actions, while ferritin alone does not show any cytotoxic activity. Since AF is able to overcome cisplatin resistance in A2780 cisplatin resistant cells (A2780cis) [9], we also evaluated the cytotoxic activity of HuHf@AF in A2780cis. The results are reported in Fig. 5. For comparison purposes the obtained IC_{50} values for cisplatin and free AF are also provided; HuHf@AF overcomes cisplatin resistance even more efficiently than free AF. Also in this case apo-HuHf does not show any cytotoxicity. This is clearly shown in Fig. 5D where an MTT time course (24, 48 and 72 h) was performed treating A2780cis cells with cisplatin, AF and HuHf@AF with the respective 72 h-IC_{50} values, while for apo-HuHf the same protein concentration as HuHf@AF was employed.

3.5. NMR metabolomics

Then, the cellular effects of HuHf@AF were investigated via ^{1}H NMR metabolomics [31,44] and the results compared with those obtained with free AF. The possible contribution to metabolomic changes of the ferritin nanocage itself was investigated by performing analogous experiments on cells treated with apo-HuHf alone. To this purpose ^{1}H NMR is applied as an untargeted approach to monitor the changes occurring upon treatment at the level of both the endo- and the exo-metabolome

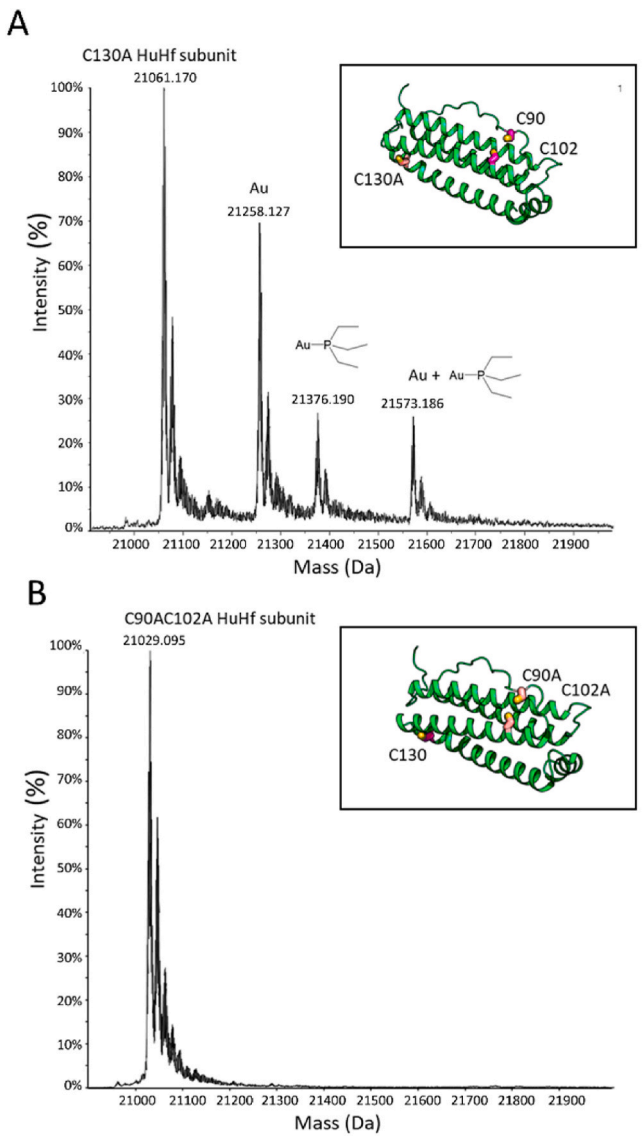

C

	Eq. of Au(I) per subunit	Au(I) per cage
WT HuHf@AF	10	13.8
C130A HuHf@AF	10	10.72
C90AC102A HuHf@AF	10	n.d.

Fig. 3. Deconvoluted ESI MS spectra of auranofin bioconjugate with A) C130A HuHf mutant (C130A HuHf@AF); B) C90AC102A HuHf mutant (C90AC102A HuHf@AF). C) Results from the ICP-OES analysis; n.d. = under the detection limit.

[16,45–48]. In the former case, NMR of cell lysates allows the quantification of about 30 intracellular metabolites (listed in Table S2), which are reporters of main metabolic pathways (glycolysis, Krebs cycle, amino acid metabolism, etc.). In the latter case, instead, the NMR spectra provide a complementary picture reporting the exchange of small molecules between the media and the cells in terms of molecules uptaken by cells from the culture medium (whose concentration in the medium decreases upon treatment) or molecules released into it (whose concentration in the medium increases upon treatment) (Table S3). Here, A2780 cells were treated with a concentration of AF and HuHf@AF equal to their respective IC_{50} values at 72 h, in such a way to work under equitoxic conditions. For each experiment, the actual gold concentration was determined by ICP-OES. For the control treatment with apo-HuHf alone, the same ferritin concentration as in the corresponding experiments with HuHf@AF was used for the analysis. A2780 cells were grown in the standard RPMI1640 medium supplemented with 2 mM glutamine and 10% of FCS. The cells were treated with AF, HuHf@AF or apo-HuHf for 24 h in order to detect, predominantly, the metabolic derangements taking place before the occurrence of significant apoptosis. A general overview of the metabolomic profiles of the cells was obtained by the score plot of the unsupervised PCA analysis (Fig. S5), that allows us to rapidly visualize the strong remodeling of the metabolomic fingerprint of A2780 cells upon AF and HuHf@AF treatments, both in the endo- and the exo-metabolome. From the score plot it is also evident that the treatment with apo-HuHf does not significantly alter the A2780 cellular metabolomic fingerprint.

The cellular metabolic changes produced by HuHf@AF are broadly consistent with the metabolic alterations previously described for A2780 cells upon free AF treatment [16] (Fig. 4D and E); in particular, we refer to a very large increase of glutathione, as the most striking intracellular alteration; modest but significant changes in Krebs cycle activity, acidification and lactate production, and glycolysis were also observed. Interestingly, the detected cellular changes induced by HuHf@AF are even more marked than those observed with free AF. The increase of intracellular glutathione is very important (about 45% larger than the increase induced by free AF) and, as in the case of free AF, it is accompanied by changes in the concentration of its amino acid constituents. Indeed, upon HuHf@AF and/or AF treatment, a greater consumption of intracellular Gly is detected along with a decrease of its excretion into the media; a greater uptake of cystine (as a source of Cys) from the medium is also monitored. Glutamine uptake is not significantly affected by the treatments. Intracellular glutamine is instead significantly lower in the treated cells, as it is used as a source of glutamate for GSH synthesis and anaplerosis. Also, the AF-induced decreased levels of intracellular asparagine and aspartate could be associated with increased anaplerotic reactions to feed the Krebs cycle that may be kept constant despite the large production of glutathione.

Among the intermediates of the Krebs cycle, a significant increase in intracellular succinate is observed after both AF and HuHf@AF treatments. Alterations in the glycolysis are also highlighted by the significant increased concentration of intracellular lactate, increased release of lactate and decreased release of pyruvate as well as increased uptake of glucose from the medium.

Importantly, apart from a moderate increase in intracellular UDP-galactose levels and a higher citrate excretion, no significant changes were detected in both cell lysates and growth media upon A2780 cell treatment with apo-HuHf (Fig. 4D and E).

3.6. The reaction of AF with the TrxR dodecapeptide

Results of the NMR metabolomic measurements strongly suggest that HuHf@AF possesses a mode of action substantially superimposable to free AF, ultimately leading to very similar alterations in the metabolomic profiles of treated cancer cells. As stated above, thioredoxin reductase is believed to be the primary target of AF nicely accounting for its main cellular effects. To further support the hypothesis of a roughly identical mode of action for HuHf@AF and free AF, the ability of HuHf@AF to metalate the C-terminal dodecapeptide of the selenoenzyme thioredoxin reductase was investigated through ESI MS measurements. Accordingly, a sample of HuHf@AF was reacted with the C-terminal dodecapeptide of the enzyme thioredoxin reductase bearing the catalytic Cys-Sec motif; the sample was analyzed over time by ESI MS. Results are shown in the graph below (Fig. 6). After 5 h of incubation the sample was ultrafiltered to separate the mixture of the biomolecules; then, the up and down fractions were separately analyzed by mass spectrometry. From inspection of the ESI MS spectra, it is evident that the signal of HuHf@AF rapidly decreases (Fig. S6A); conversely, a signal attributed to the gold(I) adduct of the C-terminal dodecapeptide is detected (Fig. S6B). These findings unambiguously document the

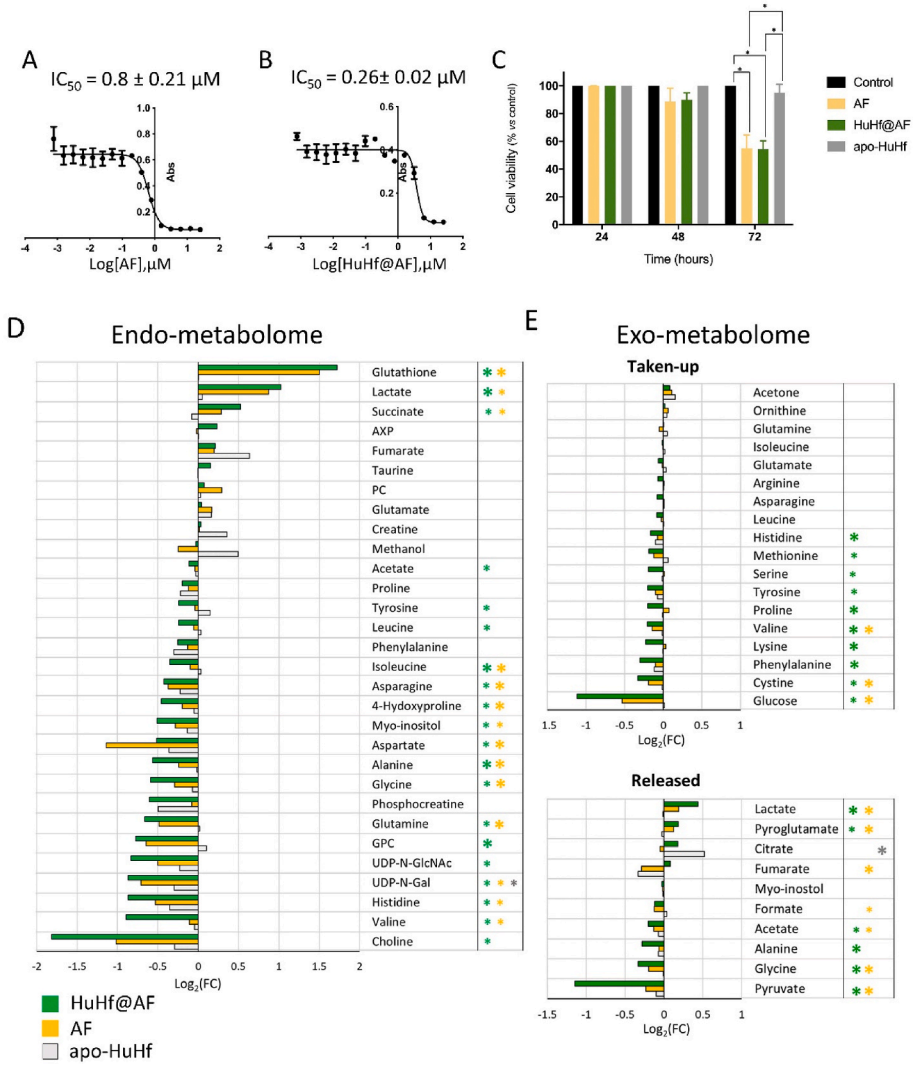

Fig. 4. A-B) Representative dose-response curves determined using MTT assay of three independent experiments performed to calculate the IC_{50} (average value ± standard deviation) of A) AF and B) HuHf@AF after 72 h on A2780 cells. C) A2780 cell viability time course assay upon treatment with AF, HuHf@AF and apo-HuHf for 24, 48 and 72 h. For AF and HuHf@AF the respective 72 h-IC_{50} values were used, while for apo-HuHf treatment, the same protein concentration as HuHf@AF was employed for the test. The histogram shows the mean and standard deviation values of the percentage of treated-A2780 viable cells relative to untreated controls *$p < 0.01$. D-E) AF, HuHf@AF and apo-HuHf-induced changes in the endo- and exo-metabolome of A2780 cells. Values of Log_2 (FC) of quantified metabolites in lysates (D) and growing media (E) for HuHf@AF, green bars, AF, yellow bars and apo-HuHf, gray bars. In panel B, the metabolites that are taken-up from the medium and those that are released into the medium are plotted separately. Metabolites with Log_2(FC) positive/negative values have higher/lower concentration in treated cells with respect to controls. Asterisks represent statistical significance: *0.05<p-value<0.01; *p-value<0.01. (For interpretation of the references to color in this figure legend, the reader is referred to the Web version of this article.)

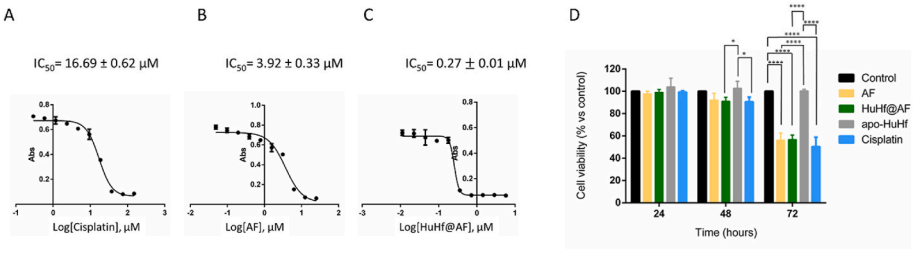

Fig. 5. A-B-C) Representative dose-response curves determined using MTT assay of two independent experiments performed to calculate the IC_{50} (average value ± standard deviation) of A) Cisplatin, B) AF and C) HuHf@AF after 72 h on A2780cis cells. D) A2780cis cell viability time course assay upon treatment with Cisplatin, AF, HuHf@AF and apo-HuHf for 24, 48 and 72 h. For cisplatin, AF and HuHf@AF the respective 72 h-IC_{50} values were used, while for apo-HuHf treatment, the same protein concentration as HuHf@AF was employed for the test. The histogram shows the mean and standard deviation values of the percentage of treated-A2780cis viable cells relative to untreated controls *$p < 0.01$ and ****$p < 0.0001$.

transfer of a gold atom from the protein to the selenopeptide. Thus, our results point out that HuHf@AF, similarly to free AF, is able to metalate effectively and quickly the selenol active site of the enzyme causing its strong inhibition.

3.7. *Insights into the mechanism of HuHf uptake and of gold release*

Literature data have established that the cellular uptake of HuHf mediated by human transferrin receptor-1, TfR1, implies HuHf import via the endosome-lysosome pathway [49]. The pH of lysosome is about 4.5 [50] and, in the case of iron-loaded ferritin, this pH drop is accompanied by the release of iron [51,52]. Here, we have used ^{19}F NMR to monitor the decrease in ferritin concentration in the growth medium as a function of time (Fig. 7). The one-dimensional ^{19}F NMR spectra of both apo and HuHf@AF show a single broad resonance centered at −125.6 ppm (referenced to trifluoroacetic acid as an external standard (0 ppm) and a linewidth of about 800 Hz. Unfortunately, and at variance with what reported [30] for thimerosal-HuHf

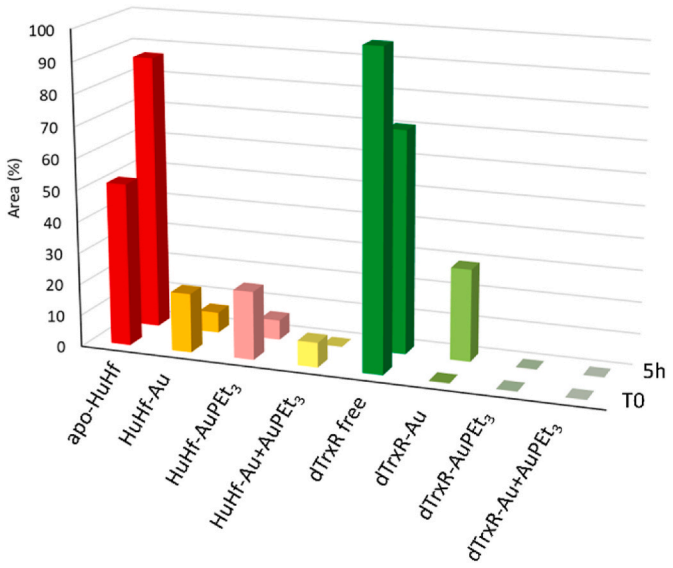

Fig. 6. Bar plots of the percentages of the areas of the ESI-MS spectra of the apo-forms and the metalated-forms of HuHf and TrxR dodecapeptide at different time points (T0 and after 5 h of incubation, T = 5 h). HuHf@AF were incubated with dTrxR at 37 °C (1:1 with respect to the gold(I) concentration per ferritin subunit, i.e. 0.4 μM). (For interpretation of the references to color in this figure legend, the reader is referred to the Web version of this article.)

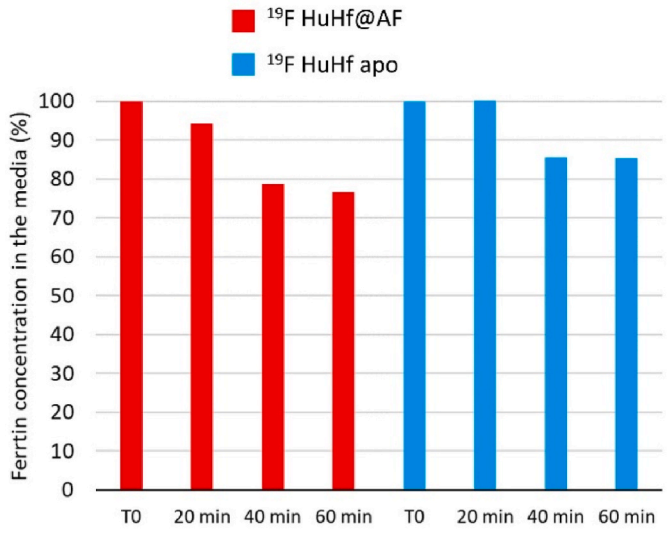

Fig. 7. Bar plot of the integrated intensities of the ^{19}F NMR signal of the apo- and the metalated-^{19}F-HuHf in A2780 cells growth media; samples were collected at different time points of incubation (T0, after 20, 40 and 60 min).

(where the free and bound form where in slow exchange on the NMR time scale), here the bound and free form are essentially indistinguishable. The integrated intensity of the resulting signal provides the overall (free and bound) amount of ferritin present in the media as a function of time of treatment; Fig. 7 clearly shows the time-dependent decrease in signal intensity in the growth media added with 10 μM ferritin cage, which accounts for an uptake of about 15–20% within the first hour of treatment. The observed trends suggest a slightly faster uptake in the case of HuHf@AF with respect to the apo-HuHf, but the differences are very minor. ^{19}F NMR could not be used to monitor the uptaken protein into the lysates because the total concentration is expected to be below the detection limit of our available NMR apparatus [30].

Finally, to simulate the conditions in the lysosome, the stability of HuHf@AF at pH 4.5 and 37 °C was evaluated by ESI-MS, which showed a significant release of gold in 24 h (Fig. S7), whereas the adduct is stable in the corresponding experiments at pH 7.4. In summary, the emerging picture is that of a quite fast internalization of HuHf (independently on the gold-load), and a possible facilitated release of the metal ion at the lysosomes level, which should further facilitate the transfer to intracellular targets like TrxR.

4. Conclusions

In conclusion, with the present study, we have demonstrated that stable, well defined and highly reproducible samples of HuHf@AF may be obtained between the gold drug AF and the ferritin nanocage on the ground of a detailed preparative procedure. Briefly, HuHf@AF is prepared through simple addition of a molar excess of AF to a solution of apoferritin followed by extensive dialysis; typically, this procedure results in the formation of a species showing an average stoichiometry of 13.8 ± 3.8 gold atoms per nanocage. ESI MS analysis reveals that gold atoms are tightly bound to the protein subunits through formation of coordinative bonds to solvent exposed protein residues. Site directed mutagenesis experiments proved unambiguously that the gold fragment binds selectively to Cys90 and Cys102. The main protein-bound gold fragment detected in the ESI MS spectra is the $AuPEt_3$ fragment. HuHf@AF is stable upon incubation with an excess of GSH, indicating that the two spatially close Cys residues on the external protein surface provide a very strong binding site for gold. Interestingly, we have shown that HuHf@AF, on a molar basis, manifests antiproliferative properties superior to free AF toward A2780 ovarian cancer cells. In addition HuHf@AF, like free AF, is able to overcome nearly completely cisplatin resistance in A2780cis cells. In turn, NMR metabolomic studies revealed that ferritin-loaded AF produces metabolic alterations of A2780 cancer cells that are almost superimposable to those of free AF under equitoxic conditions suggesting the occurrence of similar cellular effects. Notably, ESI MS measurements documented that HuHf@AF conserves the ability of free AF to metalate the C- terminal selenopeptide of thioredoxin reductase, supporting the view that TrxR remains its main cellular target. Finally, some experiments were carried out to investigate the cellular uptake of HuHf@AF and the subsequent gold release. Preliminary evidence is gained that HuHf@AF is taken up efficiently by A2780 cancer cells and that acidification of HuHf@AF down to pH 4.5 favors progressive gold release. This latter experiment may simulate HuHf@AF acidification in the lysosomes. Overall, these results point out that the mode of action of free AF and HuHf@AF are roughly the same and that the gold moiety is released intracellularly from ferritin. On the other hand, the strong binding of AF to the ferritin nanocage, mediated by the spatially close cysteines 90 and 102, can reduce the indiscriminate reactivity of the gold center with the cysteine proteome [37,53] possibly leading to a more favorable systemic toxicity profile. These results imply that the here described bioconjugate possesses highly favorable properties making it suitable for further pharmacological investigations.

Funding

This work was supported by Fondazione Cassa di Risparmio di Firenze [project number 2020.1519]; and AIRC [project number IG2021-26169].

Author contributions

Conceptualization, L.M. and P.T.; methodology, L.C., La.M., V.G., S. C., M.S., T.G.; formal analysis, L.C., La.M., V.G., S.Z., A.G., M.M., S.C., M. S., and T.G.; investigation, L.C. La.M., V.G., S.Z., A.G., M.M., S.C., M.S. and T.G.; resources, La.M.; writing original draft, L.M., P.T., L.C., La.M, and V.G.; writing–review & editing, S.Z., A.G., M.M., S.C., M.S. and T.G.; supervision, L.M. and P.T.; funding acquisition, L.M. and P.T.

The manuscript was written through contributions of all authors. All authors have given approval to the final version of the manuscript.

Declaration of competing interest

The authors declare that they have no known competing financial interests or personal relationships that could have appeared to influence the work reported in this paper.

Data availability

Data will be made available on request.

Acknowledgment

P.T., V.G., L.C. and S.Z. acknowledge the support and the use of resources of Instruct-ERIC, a Landmark ESFRI project, and specifically the CERM/CIRMMP Italy Centre. The publication was made with the contribution of the researcher Silvia Ciambellotti with a research contract co-funded by the European Union - PON Research and Innovation 2014–2020 in accordance with Article 24, paragraph 3a), of Law No. 240 of December 30, 2010, as amended, and Ministerial Decree No. 1062 of August 10, 2021. S.Z. contributed to this work before the start of his PhD.

Appendix A. Supplementary data

Supplementary data to this article can be found online at https://doi.org/10.1016/j.jddst.2023.104822.

References

[1] S. Nobili, E. Mini, I. Landini, C. Gabbiani, A. Casini, L. Messori, Gold compounds as anticancer agents: chemistry, cellular pharmacology, and preclinical studies: gold compounds as anticancer agents, Med. Res. Rev. 30 (2010) 550–580, https://doi.org/10.1002/med.20168.

[2] C.F. Shaw, Gold-based therapeutic agents, Chem. Rev. 99 (1999) 2589–2600, https://doi.org/10.1021/cr980431o.

[3] C. Roder, M.J. Thomson, Auranofin: repurposing an old drug for a golden new age, Drugs R 15 (2015) 13–20, https://doi.org/10.1007/s40268-015-0083-y.

[4] R. Rubbiani, I. Kitanovic, H. Alborzinia, S. Can, A. Kitanovic, L.A. Onambele, M. Stefanopoulou, Y. Geldmacher, W.S. Sheldrick, G. Wolber, A. Prokop, S. Wölfl, I. Ott, Benzimidazol-2-ylidene gold(I) complexes are thioredoxin reductase inhibitors with multiple antitumor properties, J. Med. Chem. 53 (2010) 8608–8618, https://doi.org/10.1021/jm100801e.

[5] W. Walther, D. Althagafi, D. Curran, C. O'Beirne, C. Mc Carthy, I. Ott, U. Basu, B. Büttner, A. Sterner-Kock, H. Müller-Bunz, G. Sánchez-Sanz, X. Zhu, M. Tacke, In-vitro and in-vivo investigations into the carbene-gold anticancer drug candidates NHC*-Au-SCSNMe2 and NHC*-Au-S-GLUC against advanced prostate cancer PC3, Anti Cancer Drugs 31 (2020) 672–683, https://doi.org/10.1097/CAD.0000000000000930.

[6] R. Rubbiani, S. Can, I. Kitanovic, H. Alborzinia, M. Stefanopoulou, M. Kokoschka, S. Mönchgesang, W.S. Sheldrick, S. Wölfl, I. Ott, Comparative in vitro evaluation of N-heterocyclic carbene gold(I) complexes of the benzimidazolylidene type, J. Med. Chem. 54 (2011) 8646–8657, https://doi.org/10.1021/jm201220n.

[7] Y. Lu, X. Ma, X. Chang, Z. Liang, L. Lv, M. Shan, Q. Lu, Z. Wen, R. Gust, W. Liu, Recent development of gold(i) and gold(iii) complexes as therapeutic agents for cancer diseases, Chem. Soc. Rev. 51 (2022) 5518–5556, https://doi.org/10.1039/D1CS00933H.

[8] C.-M. Che, R.W.-Y. Sun, Therapeutic applications of gold complexes: lipophilic gold (iii) cations and gold(i) complexes for anti-cancer treatment, Chem. Commun. 47 (2011) 9554, https://doi.org/10.1039/c1cc10860c.

[9] I. Landini, L. Massai, D. Cirri, T. Gamberi, P. Paoli, L. Messori, E. Mini, S. Nobili, Structure-activity relationships in a series of auranofin analogues showing remarkable antiproliferative properties, J. Inorg. Biochem. 208 (2020), 111079, https://doi.org/10.1016/j.jinorgbio.2020.111079.

[10] A. Bindoli, M.P. Rigobello, G. Scutari, C. Gabbiani, A. Casini, L. Messori, Thioredoxin reductase: a target for gold compounds acting as potential anticancer drugs, Coord. Chem. Rev. 253 (2009) 1692–1707, https://doi.org/10.1016/j.ccr.2009.02.026.

[11] F.H. Abdalbari, C.M. Telleria, The gold complex auranofin: new perspectives for cancer therapy, Discov. Oncol. 12 (2021) 42, https://doi.org/10.1007/s12672-021-00439-0.

[12] C. Zoppi, L. Messori, A. Pratesi, ESI MS studies highlight the selective interaction of Auranofin with protein free thiols, Dalton Trans. 49 (2020) 5906–5913, https://doi.org/10.1039/D0DT00283F.

[13] X. Zhang, K. Selvaraju, A.A. Saei, P. D'Arcy, R.A. Zubarev, E.S.J. Arnér, S. Linder, Repurposing of auranofin: thioredoxin reductase remains a primary target of the drug, Biochimie 162 (2019) 46–54, https://doi.org/10.1016/j.biochi.2019.03.015.

[14] A.A. Saei, H. Gullberg, P. Sabatier, C.M. Beusch, K. Johansson, B. Lundgren, P. I. Arvidsson, E.S.J. Arnér, R.A. Zubarev, Comprehensive chemical proteomics for target deconvolution of the redox active drug auranofin, Redox Biol. 32 (2020), 101491, https://doi.org/10.1016/j.redox.2020.101491.

[15] M. Kupiec, A. Tomaszewska, W. Jakubczak, M. Haczyk-Więcek, K. Pawlak, Speciation analysis highlights the interactions of auranofin with the cytoskeleton proteins of lung cancer cells, Pharmaceuticals 15 (2022) 1285, https://doi.org/10.3390/ph15101285.

[16] V. Ghini, T. Senzacqua, L. Massai, T. Gamberi, L. Messori, P. Turano, NMR reveals the metabolic changes induced by auranofin in A2780 cancer cells: evidence for glutathione dysregulation, Dalton Trans. 50 (2021) 6349–6355, https://doi.org/10.1039/D1DT00750E.

[17] G. Chiappetta, T. Gamberi, F. Faienza, X. Limaj, S. Rizza, L. Messori, G. Filomeni, A. Modesti, J. Vinh, Redox proteome analysis of auranofin exposed ovarian cancer cells (A2780), Redox Biol. 52 (2022), 102294, https://doi.org/10.1016/j.redox.2022.102294.

[18] Z. Wang, H. Gao, Y. Zhang, G. Liu, G. Niu, X. Chen, Functional ferritin nanoparticles for biomedical applications, Front. Chem. Sci. Eng. 11 (2017) 633–646, https://doi.org/10.1007/s11705-017-1620-8.

[19] R.R. Crichton, J.-P. Declercq, X-ray structures of ferritins and related proteins, Biochim. Biophys. Acta Gen. Subj. 1800 (2010) 706–718, https://doi.org/10.1016/j.bbagen.2010.03.019.

[20] X. Liu, E.C. Theil, Ferritins: dynamic management of biological iron and oxygen chemistry, Acc. Chem. Res. 38 (2005) 167–175, https://doi.org/10.1021/ar0302336.

[21] C. Pozzi, F. Di Pisa, C. Bernacchioni, S. Ciambellotti, P. Turano, S. Mangani, Iron binding to human heavy-chain ferritin, Acta Crystallogr. D 71 (2015) 1909–1920, https://doi.org/10.1107/S1399004715013073.

[22] C. Pozzi, F. Di Pisa, D. Lalli, C. Rosa, E. Theil, P. Turano, S. Mangani, Time-lapse anomalous X-ray diffraction shows how Fe $^{2+}$ substrate ions move through ferritin protein nanocages to oxidoreductase sites, Acta Crystallogr. D Biol. Crystallogr. 71 (2015) 941–953, https://doi.org/10.1107/S1399004715002333.

[23] B. Chandramouli, C. Bernacchioni, D. Di Maio, P. Turano, G. Brancato, Electrostatic and structural bases of Fe2+ translocation through ferritin channels, J. Biol. Chem. 291 (2016) 25617–25628, https://doi.org/10.1074/jbc.M116.748046.

[24] C. Bernacchioni, V. Ghini, E.C. Theil, P. Turano, Modulating the permeability of ferritin channels, RSC Adv. 6 (2016) 21219–21227, https://doi.org/10.1039/C5RA25056K.

[25] Z. Yang, X. Wang, H. Diao, J. Zhang, H. Li, H. Sun, Z. Guo, Encapsulation of platinum anticancer drugs by apoferritin, Chem. Commun. (2007) 3453, https://doi.org/10.1039/b705326f.

[26] R. Xing, X. Wang, C. Zhang, Y. Zhang, Q. Wang, Z. Yang, Z. Guo, Characterization and cellular uptake of platinum anticancer drugs encapsulated in apoferritin, J. Inorg. Biochem. 103 (2009) 1039–1044, https://doi.org/10.1016/j.jinorgbio.2009.05.001.

[27] D.M. Monti, G. Ferraro, A. Merlino, Ferritin-based anticancer metallodrug delivery: crystallographic, analytical and cytotoxicity studies, Nanomed. Nanotechnol. Biol. Med. 20 (2019), 101997, https://doi.org/10.1016/j.nano.2019.04.001.

[28] G. Ferraro, D.M. Monti, A. Amoresano, N. Pontillo, G. Petruk, F. Pane, M. A. Cinellu, A. Merlino, Gold-based drug encapsulation within a ferritin nanocage: X-ray structure and biological evaluation as a potential anticancer agent of the Auoxo3-loaded protein, Chem. Commun. 52 (2016) 9518–9521, https://doi.org/10.1039/C6CC02516A.

[29] R. Lucignano, A. Pratesi, P. Imbimbo, D.M. Monti, D. Picone, L. Messori, G. Ferraro, A. Merlino, Evaluation of auranofin loading within ferritin nanocages, IJMS 23 (2022), 14162, https://doi.org/10.3390/ijms232214162.

[30] L. Cosottini, S. Zineddu, L. Massai, V. Ghini, P. Turano, 19F: A small probe for a giant protein, J. Inorg. Biochem. (2023), 112236, https://doi.org/10.1016/j.jinorgbio.2023.112236.

[31] A. Vignoli, V. Ghini, G. Meoni, C. Licari, P.G. Takis, L. Tenori, P. Turano, C. Luchinat, High-throughput metabolomics by 1D NMR, Angew. Chem. Int. Ed. 58 (2019) 968–994, https://doi.org/10.1002/anie.201804736.

[32] P.G. Takis, V. Ghini, L. Tenori, P. Turano, C. Luchinat, Uniqueness of the NMR approach to metabolomics, TrAC, Trends Anal. Chem. 120 (2019), 115300, https://doi.org/10.1016/j.trac.2018.10.036.

[33] L. Conti, S. Ciambellotti, G.E. Giacomazzo, V. Ghini, L. Cosottini, E. Puliti, M. Severi, E. Fratini, F. Cencetti, P. Bruni, B. Valtancoli, C. Giorgi, P. Turano, Ferritin nanocomposites for the selective delivery of photosensitizing ruthenium-polypyridyl compounds to cancer cells, Inorg. Chem. Front. 9 (2022) 1070–1081, https://doi.org/10.1039/D1QI01268A.

[34] G. Jutz, P. van Rijn, B. Santos Miranda, A. Böker, Ferritin: a versatile building block for bionanotechnology, Chem. Rev. 115 (2015) 1653–1701, https://doi.org/10.1021/cr400011b.

[35] J. Zhang, Z. Zhang, M. Jiang, S. Li, H. Yuan, H. Sun, F. Yang, H. Liang, Developing a novel gold(III) agent to treat glioma based on the unique properties of apoferritin nanoparticles: inducing lethal autophagy and apoptosis, J. Med. Chem. 63 (2020) 13695–13708, https://doi.org/10.1021/acs.jmedchem.0c01257.

[36] L. Massai, S. Ciambellotti, L. Cosottini, L. Messori, P. Turano, A. Pratesi, Direct detection of iron clusters in L ferritins through ESI-MS experiments, Dalton Trans. 50 (2021) 16464–16467, https://doi.org/10.1039/D1DT03106F.

[37] M.S. Iqbal, S.G. Taqi, M. Arif, M. Wasim, M. Sher, In Vitro distribution of gold in serum proteins after incubation of sodium aurothiomalate and auranofin with

human blood and its pharmacological significance, Biol. Trace Elem. Res. 130 (2009) 204–209, https://doi.org/10.1007/s12011-009-8330-0.
[38] J. Talib, J.L. Beck, S.F. Ralph, A mass spectrometric investigation of the binding of gold antiarthritic agents and the metabolite [Au(CN)2]− to human serum albumin, J. Biol. Inorg. Chem. 11 (2006) 559–570, https://doi.org/10.1007/s00775-006-0103-z.
[39] D. Cirri, M.G. Fabbrini, L. Massai, S. Pillozzi, A. Guerri, A. Menconi, L. Messori, T. Marzo, A. Pratesi, Structural and solution chemistry, antiproliferative effects, and serum albumin binding of three pseudohalide derivatives of auranofin, Biometals 32 (2019) 939–948, https://doi.org/10.1007/s10534-019-00224-1.
[40] B. Maity, S. Abe, T. Ueno, Observation of gold sub-nanocluster nucleation within a crystalline protein cage, Nat. Commun. 8 (2017), 14820, https://doi.org/10.1038/ncomms14820.
[41] D.M. Monti, G. Ferraro, G. Petruk, L. Maiore, F. Pane, A. Amoresano, M.A. Cinellu, A. Merlino, Ferritin nanocages loaded with gold ions induce oxidative stress and apoptosis in MCF-7 human breast cancer cells, Dalton Trans. 46 (2017) 15354–15362, https://doi.org/10.1039/C7DT02370G.
[42] C. Kannengiesser, A.-M. Jouanolle, G. Hetet, A. Mosser, F. Muzeau, D. Henry, E. Bardou-Jacquet, M. Mornet, P. Brissot, Y. Deugnier, B. Grandchamp, C. Beaumont, A new missense mutation in the L ferritin coding sequence associated with elevated levels of glycosylated ferritin in serum and absence of iron overload, Haematologica 94 (2009) 335–339, https://doi.org/10.3324/haematol.2008.000125.
[43] W. Wang, M.A. Knovich, L.G. Coffman, F.M. Torti, S.V. Torti, Serum ferritin: past, present and future, Biochim. Biophys. Acta 1800 (2010) 760–769, https://doi.org/10.1016/j.bbagen.2010.03.011.
[44] Z. Eraslan, M. Cascante, U.L. Günther, Metabolomics in cell biology, in: V. Ghini, K. A. Stringer, C. Luchinat (Eds.), Metabolomics and its Impact on Health and Diseases, Springer International Publishing, Cham, 2022, pp. 181–207, https://doi.org/10.1007/164_2022_619.
[45] V. Ghini, F. Magherini, L. Massai, L. Messori, P. Turano, Comparative NMR metabolomics of the responses of A2780 human ovarian cancer cells to clinically established Pt-based drugs, Dalton Trans. 51 (2022) 12512–12523, https://doi.org/10.1039/D2DT02068H.
[46] V. Ghini, M. Mannelli, L. Massai, A. Geri, S. Zineddu, T. Gamberi, L. Messori, P. Turano, The effects of two cytotoxic gold(i) carbene compounds on the metabolism of A2780 ovarian cancer cells: mechanistic inferences through NMR analysis, RSC Adv. 13 (2023) 21629–21632, https://doi.org/10.1039/D3RA04032A.
[47] G. D'Alessandro, D. Quaglio, L. Monaco, C. Lauro, F. Ghirga, C. Ingallina, M. De Martino, S. Fucile, A. Porzia, M.A. Di Castro, F. Bellato, F. Mastrotto, M. Mori, P. Infante, P. Turano, S. Salmaso, P. Caliceti, L. Di Marcotullio, B. Botta, V. Ghini, C. Limatola, 1H-NMR metabolomics reveals the Glabrescione B exacerbation of glycolytic metabolism beside the cell growth inhibitory effect in glioma, Cell Commun. Signal. 17 (2019) 108, https://doi.org/10.1186/s12964-019-0421-8.
[48] V. Ghini, M. Di Nunzio, L. Tenori, V. Valli, F. Danesi, F. Capozzi, C. Luchinat, A. Bordoni, Evidence of a DHA signature in the lipidome and metabolome of human hepatocytes, IJMS 18 (2017) 359, https://doi.org/10.3390/ijms18020359.
[49] L. Li, C.J. Fang, J.C. Ryan, E.C. Niemi, J.A. Lebrón, P.J. Björkman, H. Arase, F. M. Torti, S.V. Torti, M.C. Nakamura, W.E. Seaman, Binding and uptake of H-ferritin are mediated by human transferrin receptor-1, Proc. Natl. Acad. Sci. U.S.A. 107 (2010) 3505–3510, https://doi.org/10.1073/pnas.0913192107.
[50] J. Huotari, A. Helenius, Endosome maturation: endosome maturation, EMBO J. 30 (2011) 3481–3500, https://doi.org/10.1038/emboj.2011.286.
[51] J.C. Cutrin, D. Alberti, C. Bernacchioni, S. Ciambellotti, P. Turano, C. Luchinat, S. G. Crich, S. Aime, Cancer cell death induced by ferritins and the peculiar role of their labile iron pool, Oncotarget 9 (2018) 27974–27984, https://doi.org/10.18632/oncotarget.25416.
[52] D. Sala, S. Ciambellotti, A. Giachetti, P. Turano, A. Rosato, Investigation of the iron (II) release mechanism of human H-ferritin as a function of pH, J. Chem. Inf. Model. 57 (2017) 2112–2118, https://doi.org/10.1021/acs.jcim.7b00306.
[53] J.D. Herrlinger, C. Alsen, R. Beress, U. Hecker, W. Weikert, Distribution of gold in serum erythrocytes and white blood cells after in vitro incubation and during chrysotherapy with different gold compounds, J. Rheumatol. Suppl. 8 (1982) 81–89.